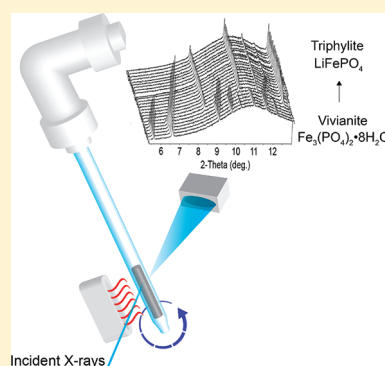# In Situ Hydrothermal Synthesis of LiFePO$_4$ Studied by Synchrotron X-ray Diffraction

Jiajun Chen,[*,†] Jianming Bai,[‡] Haiyan Chen,[§] and Jason Graetz[†]

[†]Sustainable Energy Technologies Department, Brookhaven National Laboratory, Upton, New York 11973, United States
[‡]Oak Ridge National Laboratory, Oak Ridge, Tennessee 37831, United States
[§]Physics Department, New Jersey Institute of Technology, Newark, New Jersey 07102, United States

Ⓢ *Supporting Information*

ABSTRACT: The development of high capacity, safe lithium battery materials requires new tools to better understand how reaction conditions affect nucleation and crystallization, particle size, morphology, and defects. We present a general approach for studying the synthesis of Li battery electrode materials in real time. The formation of LiFePO$_4$ was investigated by time-resolved in situ synchrotron X-ray diffraction under hydrothermal conditions, and the reaction kinetics were determined by changes of the Bragg reflections. We provide the first evidence in support of a dissolution−reprecipitation process for the formation of LiFePO$_4$, which occurs at temperatures as low as 105 °C and appears to be a three-dimensional diffusion-controlled process. Lattice parameters and their evolution were monitored in situ, as well as the formation of antisite defects and their subsequent elimination under various synthesis conditions. The ability to characterize and tailor synthesis reactions in situ is essential for rapid optimization of the synthesis procedures and, ultimately, the development of new battery electrodes.

SECTION: Energy Conversion and Storage

Concerns over global climate change and energy independence have motivated an interest in improved battery materials, driven by a change toward alternative forms of transportation, such as plug-in hybrid electric vehicles (PHEVs) and all electric vehicles (EVs), along with renewable (often intermittent) sources of energy (e.g., solar and wind).[1,2] Present-day Li-ion battery technology offers promise for meeting the electrical energy storage demands for both mobile and stationary applications. A key hurdle for the widespread commercialization of many candidate electrode materials lies in developing an economical manufacturing process. A low temperature, soft chemistry route, such as hydrothermal, is efficient, inexpensive, and sufficiently flexible so that the material's properties (e.g., cation distribution, particle size, and morphology) can be generally tailored by the synthesis conditions. However, little is known about the overall reaction pathways, the formation of intermediate phases, and exactly how the material properties are affected by the synthesis conditions. Thus, optimizing the hydrothermal procedure rests upon a tedious, time-consuming Edisonian process. Conventional hydrothermal synthesis is carried out in a sealed reactor; hence, phase identification can only take place after the reactor has cooled to room temperature and the contents are removed. Furthermore, the product must be recovered from solution, washed to remove any surface impurities, and filtered; thereafter, the filtrate cake must be dried for several hours in an oven. These ex situ experiments are not only tedious, but also make it difficult to identify the real composition of any intermediates that form during the reaction.

Recent advances in transmission electron microscopy (TEM) allow some in situ characterization of the electrode materials formed via solid-state synthesis[3] or simplified electrochemical cycling.[4] However, electron microscopy-based techniques are best suited for investigations of very localized regions of a sample, and issues with beam damage and the high vacuum requirements make it difficult to use these techniques to study wet-chemistry processes. X-ray diffraction (XRD) has proven to be a powerful technique for acquiring a fundamental understanding of structure and phase transformations. The high energy-flux of synchrotron radiation offers opportunities for studying changes in the structure and properties of complex systems in real time, e.g., in a pressurized hydrothermal environment. Due to the complexity of in situ hydrothermal configurations, only a few wet-chemistry synchrotron studies have been performed, and most have focused on phase transformations. However, the low signal-to-noise ratio and poor resolution in these studies made it difficult to obtain detailed crystallographic information.[5]

Hydrothermally prepared LiFePO$_4$ is typically plagued by a high concentration (5−7%) of antisite defects (e.g., Fe on Li sites).

Since Li$^+$ ion diffusion in LiFePO$_4$ typically occurs along one-dimensional channels, the presence of Fe on Li sites prevents lithium transport in that channel, reducing the electrode capacity and rate capability. Overall Li$^+$ ion mobility and the reactivity of the material is greatly reduced by iron disorder, as evidenced both experimentally and theoretically.[6−9]

The antisite defects in hydrothermally prepared LiFePO$_4$ can be eliminated by preparing the material at elevated temperature (>200 °C) or by including a postsynthesis, high-temperature heat treatment (600−700 °C). With the addition of carbon coatings or nanotubes, the defect-free LiFePO$_4$ exhibits excellent electrochemical performance.[6,10] In recent years there has been much interest in optimizing the hydrothermal synthesis condition for the preparation of LiFePO$_4$;[11−13] however, a number of uncertainties remain. For example, it is still not known whether LiFePO$_4$ is precipitated directly at elevated temperatures or formed after the solution has cooled. Other questions include the general solubility of LiFePO$_4$ at high temperatures during the reaction, the formation of intermediates between the reactant and product, crystal growth rate, and the amount of structural disorder in the final product. Answers to all of these questions are necessary to improve the synthesis procedure and reduce the total energy requirement. An especially important problem is that of the relationship between the concentration of defects (primarily antisite defects) and the temperature and time of synthesis. Both experimental and theoretical studies have shown that limiting the number of channel-blocking point defects (iron on lithium sites) is critical for the preparation of LiFePO$_4$ suitable for lithium-ion batteries. Currently, little is known about how the defect concentration changes during synthesis and how to control it.[14] Recently, we tracked the antisite defect concentration in hydrothermally prepared LiFePO$_4$ in real time during a post synthesis heat treatment.[15] Time-resolved, synchrotron XRD revealed that antisite defects are completely eliminated above 500 °C, substantially lower than the previously reported value of 700 °C. A significant enhancement in the electrochemical capacity was observed with the defect-free material, with the specific capacity increasing by approximately 60%.

Although a postsynthesis heat treatment is effective at eliminating defects, a one-pot procedure is likely to be much more cost-effective for manufacturing defect-free LiFePO$_4$. Here we present our general approach for studying the formation of olivine LiFePO$_4$ by time-resolved in situ synchrotron XRD under hydrothermal conditions. These data offer new insights into the hydrothermal synthesis of olivine electrode materials. For the first time, we achieved a one-pot in situ hydrothermal synthesis of olivine LiFePO$_4$ that revealed the formation and elimination of antisite defects in real time. The experimental methodology we introduce affords a general solution for obtaining a more fundamental understanding of the correlation between synthesis conditions, crystallization processes, and the properties that will lead to rational design of advanced lithium-electrode materials.

To study the formation of olivine LiFePO$_4$, we developed a sealed quartz tube to serve as an in situ hydrothermal reactor, as shown in Figure 1a. Rather than prepressurizing the reactor at room temperature, similar to previous in situ studies,[5] in our experiments the reactor pressure was allowed to increase with temperature (autogenous pressure), which more closely resembles the conditions used in autoclaves (e.g., Parr reactor) during standard hydrothermal syntheses. The sealed reactor was rotated continuously during the XRD measurements, which ensures the slurry is well mixed and also minimizes effects of preferred
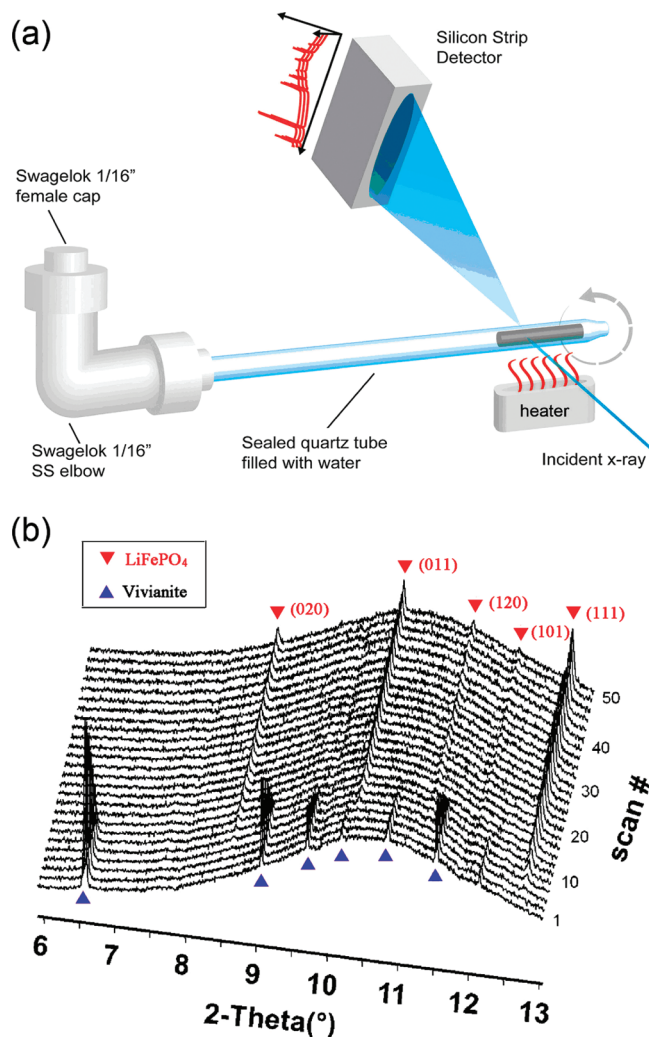

Figure 1. (a) An illustration of the in situ hydrothermal reactor. (b) Time-resolved XRD patterns during the transformation of vivianite to LiFePO$_4$ at 105 °C. (XRD patterns were collected with an X-ray wavelength of λ = 0.7748 Å at ~1 min/pattern; for clarity, every two scans were plotted).

orientation, thereby providing an averaged XRD pattern better suited for quantitative analysis (Rietveld refinement). Ferrous sulfate (0.695 g), 1 M phosphoric acid (~2.5 mL), and lithium hydroxide (0.315 g) were mixed together to form a greenish slurry, which was immediately injected into the quartz capillary. A high-resolution XRD pattern was acquired immediately after injection at 30 °C. The precursor phase, shown in Figure S1 (Supporting Information), was clearly indexed as Fe$_3$(PO$_4$)$_2$· 8H$_2$O, vivianite (PDF# 30-0662), which is in contrast to Qin et al.'s previous observations of Li$_3$PO$_4$ and Li$_2$SO$_4$·H$_2$O phases under essentially identical conditions.[16] Rietveld refinement of the powder XRD pattern indicated it was monoclinic, $C12/m1$ space group, with a = 10.1028(3) Å, b = 13.4392(5) Å, c = 4.7104(1) Å, a cell volume of 619.72(4) Å^3, and α = 90°, β = 104.304(2)°, γ = 90°. These data are in fair agreement with the mineral structure from Fejdi et al.[17]

To explore the mechanism of the LiFePO$_4$ formation in a time-resolved manner, successive diffraction patterns were taken every minute. Quantitative growth and decay curves were determined from analyzing the integrated Bragg peak intensities
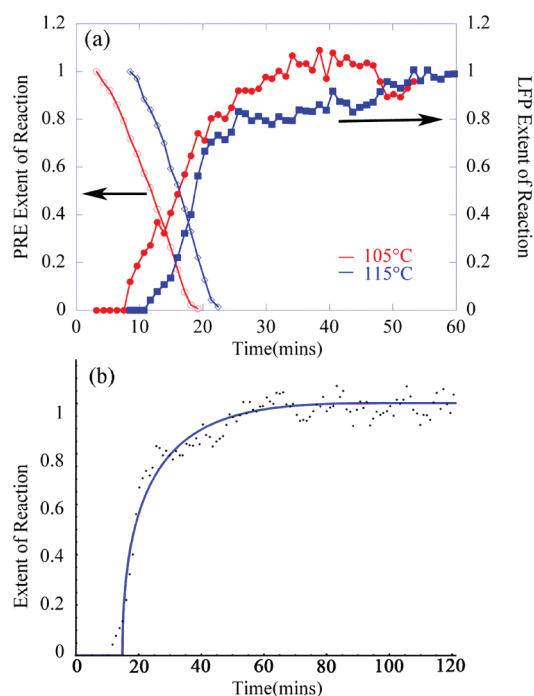
1875

dx.doi.org/10.1021/jz2008209 |J. Phys. Chem. Lett. 2011, 2, 1874−1878

Figure 2. (a) Comparison of decay curves of the vivianite precursor and the crystallization curves for $LiFePO_4$ formed at 105 and 115 °C. (b) Crystallization curve for $LiFePO_4$ formed at 115 °C and the calculated fit using the 3-D diffusion equation (blue).

Figure 3. (a) Time-resolved XRD patterns from the in situ hydrothermal synthesis of $LiFePO_4$ heated from 100 to 160 °C. XRD patterns were collected continuously at 3.5 min/pattern with an X-ray wavelength of $\lambda = 0.7748$ Å. (b) Expanded region of XRD pattern ($6-13°$ 2θ) clearly shows dissolution of vivianite and the formation of $LiFePO_4$.

of the reactants and the products. The peak intensities were extracted using an automated pseudo-Voigt profile-fitting routine from the Jade Software package. In the reactions carried out at 105 °C (shown in Figure 1b), the precursor peaks gradually decrease, disappearing after only ~17 min, suggesting complete dissolution of the vivanite. The formation of crystalline $LiFePO_4$ is initially detected ~5 min after the precursor peak intensities begin to decline. The integrated intensity of $LiFePO_4$ peaks continues to rise over the next 30 min and then remains essentially constant through the remainder of the experiment. This experiment was repeated at 115 °C.

Figure 2 shows the decay curve of the vivianite precursor and the crystallization curves for the formation of $LiFePO_4$ at 105 and 115 °C. After correcting for small changes in the incubation time (time of first detection of crystalline product), and accounting for fluctuations in the measured intensities, the rate of $LiFePO_4$ formation at the two different temperatures were found to be very similar (Figure S2).

To gain new insight into the kinetics of the crystallization reaction, the data in Figure 2 (115 °C) were fit to the Avrami–Erofe'ev equation: $\alpha = 1 - \exp[-(k(t - t_0)^n)]$, which assumes the reaction rate is determined by the nucleation and growth of the product. In this expression, t is the reaction time, t_0 is the induction time for crystallization, k is the rate constant, and n is the Avrami exponent. The best fit was achieved with an exponent of $n \sim 0.58$, although a slight deviation from this form was visible during the first few minutes of $LiFePO_4$ formation. The Avrami exponent (n) was also calculated from a Sharp–Hancock plot, which gave a value of $n = 0.64$ (Figure S3). Values of $n < 1$ are not consistent with classical Avrami kinetics, but Francis et al. have shown that particle growth, limited purely by three-dimensional (3-D) diffusion, mimics the Avrami–Erofe'ev
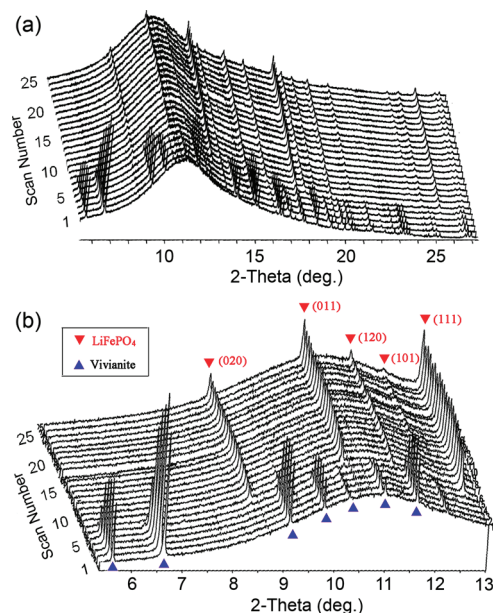
model with $n = 0.57$.[18] In the same work, the hydrothermal synthesis of microporous gallophosphate showed a weak dependence of the kinetic constants on the synthesis temperature over a range of 10–20 °C (similar to our own observations), and the best fit was achieved with an exponent of $n \sim 0.45$.[18] Motivated by these similarities, the 115 °C crystallization data was fit using a 3-D diffusion-limited growth model: $[1 - (1 - \alpha)^{1/3}]^2 = k(t - t_0)$ from $t_0 = 14.8$ s until $t = 5418$ s (in Figure 2b). On the basis of the high quality of the fit, $R^2 = 0.9974$, it is likely that a 3-D diffusion-controlled process dictates the rate of formation of $LiFePO_4$, which occurs by a typical dissolution-recrystallization process during hydrothermal synthesis.

Typically, the crystallization rate of a 3-D diffusion-controlled reaction is determined by how quickly species are transported to the nucleation sites. Once nucleation has occurred, the rate of crystallization is determined only by the rate at which species in solution can diffuse onto the nucleation site. This suggests that vigorous stirring should effectively speed up the diffusion during the reaction and possibly enhance the crystallization process of $LiFePO_4$. Since the formation of $LiFePO_4$ occurs by direct precipitation at elevated temperature, crystal growth techniques that rely on manipulating the saturation limit to control particle size may not be effective. The slow cooling of the liquid is unlikely to yield larger $LiFePO_4$ crystallites because the crystallization is already complete at the elevated temperature (before cooling).

At reaction temperatures of 100 °C and higher, both the dissolution of the precursor and the precipitation of the products is rapid, resulting in the transformation of vivianite to lithium iron phosphate over several minutes. At lower temperatures (e.g., 95 °C and below) the diffraction patterns indicate that the vivianite precursor is not completely dissolved even after a few hours. These data also indicate the complete absence of crystalline $LiFePO_4$, as well as the formation of a side product that was not identified.
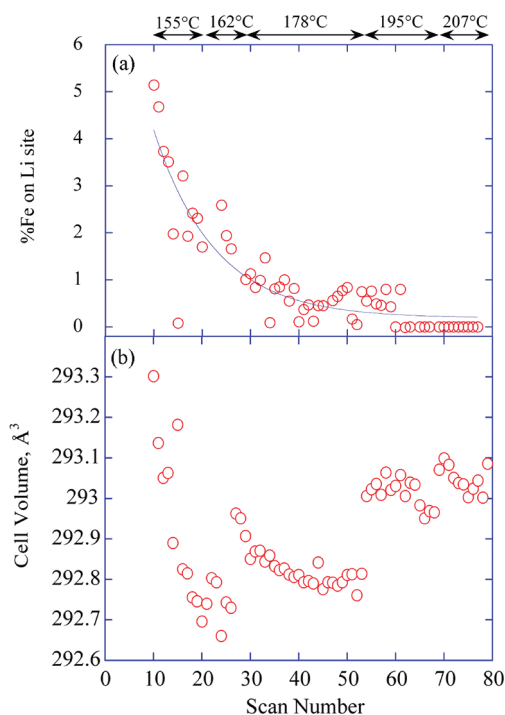
Figure 4. (a) Concentration (percent) of iron on lithium sites as a function of scan number during in situ hydrothermal synthesis from 155 to 210 °C. The average of the standard deviation of these refined atomic occupancies is around 0.4%. The blue line is present to guide the eye. (b) The unit cell volume as a function of scan number during in situ hydrothermal synthesis from 155 to 210 °C.

A series of experiments were performed at higher temperatures to study changes in the crystallographic structure. First, after injecting the precursor into the capillary, the solution was quickly heated at a rate of about 4 °C/min from room temperature up to 155 °C, and held for 45 min. Then, the temperature was raised to 178 °C, and held for 84 min. In the third step, the temperature was increased to 195 °C and held for 40 min. Finally, the sample temperature was raised to ~210 °C, and held 40 min. XRD patterns were recorded continuously after the sample temperature reached 100 °C.

The time-resolved XRD patterns from 100 to 160 °C are shown in Figure 3 (3.5 min/scan). As the temperature rises from 100 °C, the intensity of the characteristic Bragg peaks from the vivianite precursor (2θ = 5.6° (110) reflection and 6.6° (020) reflection) fall sharply. The peaks from $LiFePO_4$ appear and gradually increase during this stage, implying the coexistence of both the vivianite and tryphylite phases. At ~130 °C, the characteristic diffraction peaks from vivianite have completely disappeared, and only the peaks from $LiFePO_4$ are evident, indicating the solid precipitate is pure $LiFePO_4$.

The high angular resolution (0.005°/step) of the diffraction data obtained are well suited to Rietveld refinement analysis, which was performed for the $LiFePO_4$ patterns acquired from 155 to 210 °C. All of the diffraction peaks shift to higher angles when the temperature is increased from 155 to 178 °C, indicating a decrease of the unit cell dimensions. The initial lattice parameters of $LiFePO_4$ at 155 °C were a = 10.3632(5) Å, b = 6.0030(3) Å, c = 4.7147(2) Å with a cell volume of 293.30(4) Å^3. The refinement was terminated at reliability values of Rwp = 1.37% and Rp = 1.03%. At 178 °C the lattice parameters (before

temperature soak) were a = 10.3515(3) Å, b = 6.0119(2) Å, c = 4.7060(1) Å with a cell volume of 292.87(2) Å^3. The refinement was terminated at a reliability of Rwp =1.66% and Rp = 1.32%.

The time-resolved crystallographic information, including the cell volumes and the antisite defect concentration (Fe on Li sites) determined from Rietveld refinement, are shown in Figure 4. The concentration of antisite defects as a function of the hydrothermal synthesis temperature is shown in Figure 4a. The average of the standard deviation of these refined atomic occupancies is around 0.4%. The onset of cation ordering occurs at around 155 °C with an initial concentration of Fe on Li sites of 5.1%. The antisite defect concentration drops by ~1.7% after holding at 155 °C for about 45 min. The concentration of iron on lithium sites continues to decline with increasing temperature. At 178 °C (before holding), the defect concentration is about 1%, and this value drops to between 0.5% and 0.8% after holding at this temperature for 40 min. The number of antisite defects abruptly drops to zero when the temperature reaches ~195 °C, even without the temperature soak.

Normally, when heated, $LiFePO_4$ exhibits an increase in the unit cell dimensions due to thermal expansion; however, here we see the opposite effect. Our findings clearly reveal a competition between thermal expansion and cation ordering, which results in a contraction of the unit cell. The lattice parameters of $LiFePO_4$ at 210 °C before holding were a = 10.3519(2) Å, b = 6.0153(2) Å, c = 4.7060(1) Å with a cell volume of 293.04(2) Å^3. The refinement was terminated at a reliability of Rwp = 1.81% and Rp = 1.43%. As shown in Figure 4b, the majority of the antisite defects were eliminated at temperatures between 155 and 178 °C. Thus, the cell volume decreased due to the elimination of antisite defects offsetting the thermal expansion. At temperatures from 180 to 210 °C, less than 0.5% iron disorder was removed and a nearly defect-free material was obtained when the sample reached ~195 °C. After almost all of the antisite defects were removed, the thermal expansion dominates and the unit cell dimensions increase after scan #53. Once the sample was allowed to cool down to 40 °C the final lattice parameters were a = 10.3319(1) Å, b = 6.0040(1) Å, c = 4.6939(1) Å with a cell volume of 291.18(1) Å^3. The reliability factors for this fit were Rwp = 1.41% and Rp = 0.95%. The unit cell volume is consistent with the cell volume in defect-free $LiFePO_4$ (no iron on lithium sites) at room temperature, which is typically 290−291.4 Å^3.[19]

In summary, we performed a one-pot in situ hydrothermal synthesis of olivine $LiFePO_4$ and show that $LiFePO_4$ can be formed at temperatures as low as 105 °C. The formation of $LiFePO_4$ occurs by a straightforward dissolution−reprecipitation process and is controlled by 3-D diffusion. No obvious intermediate phases were formed during the synthesis, which fosters the rapid formation of olivine $LiFePO_4$ under hydrothermal conditions at low temperatures. We demonstrated the formation and elimination of antisite defects in real-time during hydrothermal synthesis and showed that the dwell time (temperature soak) plays an important role in reducing antisite defects. Given the low synthesis temperature, lack of costly and volatile solvents, and the scalability of this process, we expect this procedure will be well suited to the industrial-scale synthesis of high performance $LiFePO_4$ for lithium batteries.

The investigation of electrode synthesis reactions by in situ synchrotron XRD opens a new route to establishing correlations between synthesis conditions, crystallization processes and ultimately material properties and should lead to a more rational design of advanced materials for lithium battery electrodes. In

addition, by tracking the formation of crystalline intermediates and short-lived phases, we expect this type of technique will be helpful in the preparation of new materials, especially metastable compounds that may form as intermediates.

■ ASSOCIATED CONTENT

ⓈSupporting Information.   Additional experimental data, XRD patterns, SEM images, and Rietveld refinement results for the formation of olivine $LiFePO_4$. This material is available free of charge via the Internet at http://pubs.acs.org.

■ AUTHOR INFORMATION

Corresponding Author
*E-mail: jjchen@bnl.gov; fax: 631-344-7905; phone: 631-344-2479.

■ ACKNOWLEDGMENT

■ REFERENCES

(1) Whittingham, M. S. Materials Challenges Facing Electrical Energy Storage. *MRS Bull.* **2008**, *33*, 411–419.

(2) Kamat, P. V. Electrochemistry in the Driver's Seat. *J. Phys. Chem. Lett.* **2010**, *1*, 2220–2221.

(3) Chung, S. Y.; Kim, Y. M.; Kim, J. G.; Kim, Y. J. Multiphase transformation and Ostwald's rule of stages during crystallization of a metal phosphate. *Nat. Phys.* **2009**, *5*, 68–73.

(4) Huang, J. Y.; Zhong, L.; Wang, C. M.; Sullivan, J. P.; Xu, W.; Zhang, L. Q.; Mao, S. X.; Hudak, N. S.; Liu, X. H.; Subramanian, A.; et al. In Situ Observation of the Electrochemical Lithiation of a Single SnO_2 Nanowire Electrode. *Science* **2010**, *330*, 1515–1520.

(5) Shen, X. F.; Ding, Y. S.; Hanson, J. C.; Aindow, M.; Suib, S. L. In Situ Synthesis of Mixed-Valent Manganese Oxide Nanocrystals: An In Situ Synchrotron X-ray Diffraction Study. *J. Am. Chem. Soc.* **2006**, *128*, 4570–4571.

(6) Chen, J. J.; Whittingham, M. S. Hydrothermal Synthesis of Lithium Iron Phosphate. *Electrochem. Commun.* **2006**, *8*, 855–858.

(7) Morgan, D.; Van der Ven, A.; Ceder, G. Li Conductivity in Li_xMPO_4 (M = Mn, Fe, Co, Ni) Olivine Materials. *Electrochem. Solid-State Lett.* **2004**, *7*, A30–A32.

(8) Islam, M. S.; Driscoll, D. J.; Fisher, C. A. J.; Slater, P. R. Atomic-Scale Investigation of Defects, Dopants, and Lithium Transport in the $LiFePO_4$ Olivine-Type Battery Material. *Chem. Mater.* **2005**, *17*, 5085–5092.

(9) Malik, R.; Burch, D.; Bazant, M.; Ceder, G. Particle Size Dependence of the Ionic Diffusivity. *Nano Lett.* **2010**, *10*, 4123–4127.

(10) Lima, M. D.; Fang, S. L.; Lepro, X.; Lewis, C.; Ovalle-Robles, R.; Carretero-Gonzalez, J.; Castillo-Martinez, E.; Kozlov, M. E.; Oh, J. Y.; Rawat, N.; Haines, C. S.; et al. Biscrolling Nanotube Sheets and Functional Guests into Yarns. *Science* **2011**, *331*, 5.

(11) Ferrari, S.; Lavall, R. L.; Capsoni, D.; Quartarone, E.; Magistris, A.; Mustarelli, P.; Canton, P. Influence of Particle Size and Crystal Orientation on the Electrochemical Behavior of Carbon-Coated LiFePO_4. *J. Phys. Chem. C* **2010**, *114*, 12598–12603.

(12) Qian, J. F.; Zhou, M.; Cao, Y. L.; Ai, X. P.; Yang, H. X. Template-Free Hydrothermal Synthesis of Nanoembossed Mesoporous $LiFePO_4$ Microspheres for High-Performance Lithium-Ion Batteries. *J. Phys. Chem. C* **2010**, *114*, 3477–3482.

(13) Zhao, J. Q.; He, J. P.; Zhou, J. H.; Guo, Y. X.; Wang, T.; Wu, S. C.; Ding, X. C.; Huang, R. M.; Xue, H. R. Facile Synthesis for $LiFePO_4$ Nanospheres in Tridimensional Porous Carbon Framework for Lithium Ion Batteries. *J. Phys. Chem. C* **2011**, *115*, 2888–2894.

(14) Chung, S. Y.; Choi, S. Y.; Yamamoto, T.; Ikuhara, Y. Atomic-Scale Visualization of Antisite Defects in $LiFePO_4$. *Phys. Rev. Lett.* **2008**, *100*, 4.

(15) Chen, J. J.; Graetz, J. Study of Antisite Defects in Hydrothermally Prepared $LiFePO_4$ by in Situ X-ray Diffraction. *Appl. Mater. Interfaces* **2011**, *3*, 1380–1384.

(16) Qin, X.; Wang, X. H.; Xiang, H. M.; Xie, J.; Li, J. J.; Zhou, Y. C. Mechanism for Hydrothermal Synthesis of $LiFePO_4$ Platelets as Cathode Material for Lithium-Ion Batteries. *J. Phys. Chem. C* **2010**, *114*, 16806–16812.

(17) Fejdi, P.; Poullen, J. F.; Gasperin, M. Refinement of the Structure of Vivianite, $Fe_3(PO_4)_2 \cdot 8H_2O$. *Bull. Mineral.* **1980**, *103*, 135–138.

(18) Francis, R. J.; O'Brien, S.; Fogg, A. M.; Halasyamani, P. S.; O'Hare, D.; Loiseau, T.; Ferey, G. Time-Resolved In-Situ Energy and Angular Dispersive X-ray Diffraction Studies of the Formation of the Microporous Gallophosphate ULM-5 under Hydrothermal Conditions. *J. Am. Chem. Soc.* **1999**, *121*, 1002–1015.

(19) Chen, J. J.; Vacchio, M. J.; Wang, S. J.; Chernova, N.; Zavalij, P. Y.; Whittingham, M. S. The Hydrothermal Synthesis and Characterization of Olivines and Related Compounds for Electrochemical Applications. *Solid State Ionics* **2008**, *178*, 1676–1693.